Pergamon

Int. J. Heat Mass Transfer. Vol. 41, Nos 6–7, pp. 881–897, 1998

Printed in Great Britain
0017-9310/98 $19.00+0.00

PII: S0017-9310(97)00173-7

A multiphase formulation for fire propagation in heterogeneous combustible media

M. LARINI, F. GIROUD, B. PORTERIE and J.-C. LORAUD

Département Ecoulements Diphasiques et Réactifs, IUSTI, UMR CNRS 139, 5 rue Enrico Fermi, Technopôle de Château-Gombert, 13453, Marseille Cedex 13, France

(*Received* 2 *April* 1996 *and in final form* 4 *June* 1997)

Abstract—A general formulation based on a weighting average procedure is developed for describing the fire-induced behaviour of a multiphase, reactive and radiative medium. The complete set of the resulting equations should be used as the basic one for later studies, especially in the framework of wildland fires. For the moment, in order to demonstrate the capability of the general formulation, a simplified model, named zeroth-order model, in which some physical phenomena (such as char combustion, second-order terms, particle motion) are neglected is presented. In the frame of this simplified model, reverse and forward one-dimensional fire propagations through an heterogeneous medium composed of fixed fuel particles are studied numerically. © 1997 Elsevier Science Ltd.

1. INTRODUCTION

Fire propagation in heterogeneous combustible media is the result of both transfers between a gaseous phase (air and/or combustion products) and solid particles, and radiative heat transfer between particles. Wildland fire is typical of the combination of such phenomena.

In the present work, a general theoretical approach is proposed. Following the Weber's classification of the existing models of fire spread through fuel beds [1], our approach is to be ranked among the "physical and kinetic" models.

The present model is a multiphase, reactive, and radiative field model. A gas phase flows through N solid phases which constitute an idealized representation of the heterogeneous combustible medium. Each solid phase (called also a family) consists of particles of the same geometrical (e.g. shape, size, and arrangement) and thermochemicophysical properties, providing in this way the same behaviour under fire. Although our model can be used for a wide variety of applications, the present study is focused on the modelling of wildland fire propagation. In the present application, general problematics of forest fire is not tackled and the study is restricted to the scale of a vegetal stratum of medium thickness (litter, bush, etc.).

Many authors tried to develop generally applicable models of fire spread through fuel beds. In the very comprehensive review of Weber [1], fire spread models are discussed and classified as statistical, empirical, or physical models in accordance with the methods used in their construction. In the statistical models, the fire spread rate is predicted without involving any physical mechanisms, whereas the empirical models are based on the physical principle of conservation of energy, but do not differentiate between modes of heat transfer. In the physical models, the modes of heat transfer are differentiated and the fire spread rate along a given direction is found by solving a one dimensional steady energy equation (see, for example, Refs [2, 3]) or a bidimensional one [4]. They differ mainly owing to the heat transfer mechanisms involved in their formulation: embers radiation, flame radiation, convective transfer between the gas and solid phases, heat losses. The necessary input data are the topology of the combustible medium (density, surface area per unit volume, etc.), the thermochemical properties of the fuel material, and the ignition criteria. In addition, reduced models are developed in order to describe such phenomena as embers or flame radiation, heat losses, and convective transfer between gas and solid particles. Therefore, parameters such as the geometry of the flame (size, angle of inclination), convection heat transfer coefficient between gas and particles have to be known. These parameters are often difficult to obtain, and may vary from one situation to another. Flame shape can also be modified by the aerodynamic structure of the environment in which the fire develops, but these models are not capable of modelling such fire-aerodynamic interactions.

In the present multiphase formulation, the basic physical mechanisms and the strong coupling between the phases due to mass, momentum, energy transfers are considered. As an example, it accounts for the basic physico-chemical processes such as pyrolysis, chemical reactions in the gas phase, and embers combustion. Aerodynamic and thermal fields induced by the fire in complex situations (wind condition, terrain

NOMENCLATURE

C_p	specific heat at constant pressure
e	specific internal energy
$\mathbf{F}$	body force
L_g^{Ω}	radiant intensity
$\dot{m}$	mass flux
n	number of particles per unit volume
nesp	number of gascous species
N	number of solid phases or families
p	pressure
Pr	Prandtl number ($\mu C_p/\lambda$)
$\mathbf{q}$	heat flux vector
r	particle radius
$\mathbf{R}$	radiative flux vector
t	time
T	temperature
$\mathbf{v}_m^s$	velocity of the species s in the phase m with respect to stationary coordinate axes ($\mathbf{v}_m^s = \mathbf{v}_m + \mathbf{V}_m^s$)
$\mathbf{v}_m$	mass average velocity of the phase m
V	control volume
$\mathbf{V}_m^s$	mass diffusion velocity of the species s in the phase m
$\mathbf{v}_m^{pr}$	mass diffusion velocity of the pyrolysing or drying products in the phase m
W	molecular weight
Y_m^s	mass fraction of the chemical species s in the phase m.

Greek symbols

α_m	defined by V_m/V
Δh_{fs}^0	standard heat of formation of the species s
λ	thermal conductivity
μ	dynamic viscosity
ρ	density
ρ_k^{pr}	density of pyrolysis or drying products of the phase k
σ_k	surface to volume ratio of the phase k
σ	stress tensor
ω_m^s	mass rate of production of species s in the phase m
Ω	solid angle.

Diacriticals

$\langle\rangle$	average property
[]	source term.

Superscripts

pr	pyrolysis or drying products due to the thermal degradation of the fuel
s	species s.

Subscripts

0	initial condition
1	solid-phase or family 1
2	solid-phase or family 2
eq	equivalent multiphase model
g	phase g
i	ith coordinate direction
ign	ignition
in	inlet condition
I	solid–gas interface
k	phase k
m	phase m ($m = g$ or k)
p	particle
pyr	pyrolysis products
vap	water vapour.

slope) are attainable as well as the flame characteristics and the physical state of embers (which are no longer input data). The solution is obtained from input data which are more basic and realistic than those required in the "physical models". Information on the fuel (structure and composition, spatial heterogeneity), the topography of the terrain and atmospheric conditions are only needed.

The result of the present formulation is a complex set of coupled nonlinear equations which must be solved numerically. The solution requires significant computer resources. So, it is not reasonable at the time of the paper to consider this model as an operational tool for fire fighting (it appears to be different for fire prevention), but rather as an aid in improving the physical models which can be integrated in operational systems. However that may be, the equations for the multiphase, reactive and radiative model will be useful for modelling forest fire propagation. This will be done at the conclusion of the European project EFAISTOS on experiments and simulations for improvement of behaviour models of forest fires in 1998.

After presenting the general multiphase formulation in Section 2, a zeroth-order model based on simplifying physical assumptions (char combustion, second-order terms and particle motion are neglected) and simplified sub-models is described in Section 3. The governing equations of the zeroth-order model are solved by using the numerical procedure briefly presented in Section 4. Before concluding, the numerical results obtained from the simplified model in the case of reverse and forward configurations are discussed. The unique goal of the numerical simu-

lations performed in this paper is to demonstrate the capability of our model in taking into account the coupling of the main phenomena.

2. STATEMENT OF THE MULTIPHASE, REACTIVE AND RADIATIVE FIELD EQUATIONS

2.1. *The physical problem*

In two dimensions (x, z), fire propagation can be illustrated by the sketch shown in Fig. 1. In the present approach, the fuel bed is considered as an heterogeneous medium composed of solid particles of various kinds. In a small control volume V, N solid phases coexist with the gas phase. As explained in the Introduction, each solid phase is composed of particles having identical geometrical and physicochemical properties.

The packing ratio of the phase k is defined as

$$\alpha_k = \frac{V_k}{V} \tag{1}$$

where V_k is the volume occupied by the phase k in the volume V.

In the same way, the fractional porosity, also named void fraction or "aeration degree", is defined as

$$\alpha_g = \frac{V_g}{V}. \tag{2}$$

From these definitions, we have:

$$\alpha_g + \sum_{k=1}^{N} \alpha_k = 1. \tag{3}$$

Transfers between gas phase and each solid phases are the key concept for the understanding of the fire propagation mechanisms. These transfers are directly related to S_{gk}, the contact surface between the gas phase and each solid phase k.

For the phase k:

$$\frac{S_{gk}}{V} = \frac{V_k}{V}\frac{S_{gk}}{V_k} = \alpha_k \sigma_k \tag{4}$$

where $\sigma_k = S_{gk}/V_k$ is the surface to volume ratio of the phase k.

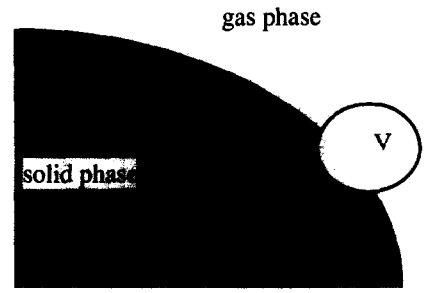

Fig. 2. Control volume V containing both gas phase and one solid phase.

Multiphase, reactive and radiative effects are included in the general formulation. For the gas phase and each solid phase, mass, momentum, and energy balance equations are derived. In addition to these equations, there is a continuity equation for each chemical species which are present in the medium. The radiative contribution to the source terms of energy equations is evaluated by solving the equation of thermal radiation intensity.

The derivation is carried out in two steps. In the first step, a small control volume containing both the gas phase and one solid phase is considered (Fig. 2). The method developed by Delhaye [5] is used to derive the local instantaneous balance equations for both phases, the chemical species continuity equations, and the associated jump conditions at the solid–gas interface surface S_{gk} $(k = 1)$. At this step, the physicochemical processes of drying and pyrolysis due to the thermal decomposition of the solid fuel are explicitly introduced. The char combustion appears implicitly through the jump conditions.

The second step is devoted to the formulation of the multiphase $(k > 1)$, reactive, and radiative field equations. The macroscopic balance equations are obtained from the local instantaneous ones by using the well-known formal averaging method. This method was first introduced by Anderson and Jackson [6], and used later by Gough and Zwarts [7] in a slightly different form. In this method, a weighting function is defined to obtain the average values of

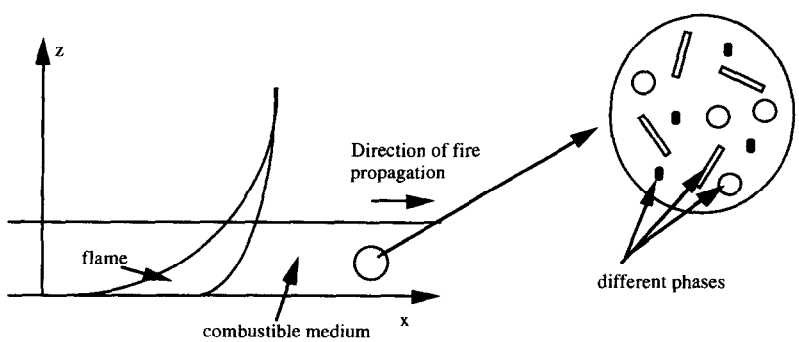

Fig. 1. Schematic representation of the physical problem.

properties. In the present formulation, following Anderson and Jackson, a weighting function is defined which depends on spatial coordinates only. A weighting function depending on both spatial coordinates and time, as suggested by Gough and Zwarts, could be used in a future theoretical development. An averaged directional equation of the radiative intensity for the multiphase medium is similarly derived.

Our approach has the benefit of a great generality. Its application to the field of wildland fires allows us to make some convenient assumptions. For example, the assumption of motionless solid particles can be reasonably utilized. For the purposes of extinguishing fires and of controlling fire growth, water sprinkling processes may be tackled by considering water as a phase k. This will be the subject of future works.

2.2. *Local instantaneous equations and jump conditions*

If contacts between solid phases are neglected, the more general situation which may occur in a small control volume V containing both the gas phase and one solid phase k may be represented schematically in Fig. 3. V is a fixed control volume in which both the two phases are allowed to move. Thus, we have

$$V = V_g(t) \bigcup V_k(t).$$

The phase k loses mass due to bulk processes that are drying and pyrolysing processes. During such phenomena, vapour and/or combustion gas migrate through the solid matrix (considered as a microporous medium), reach the interface, and then escape from the solid phase.

We begin by writing balance equations for the transport quantity ψ_m ($m = g, k$) over the control volume V and at the same time, balance equations for pyrolysis products over the control volume V_k. By combining these equations, a generic transport equation can be written as

$$\begin{aligned}\sum_m \frac{\mathrm{d}}{\mathrm{d}t}\int_{v_m} \rho_m\psi_m \,\mathrm{d}v &= -\sum_m \int_{a_m} (\rho_m\psi_m\mathbf{v}_m + \mathbf{J}_m)\cdot\mathbf{n}_m \,\mathrm{d}a \\ &+ \sum_m \int_{v_m} \rho_m\Phi_m \,\mathrm{d}v - \int_{v_k} S_k \,\mathrm{d}v \\ &+ \int_{a_{gk}^I} (\rho_k^{\mathrm{pr}}\psi_k^{\mathrm{pr}}\mathbf{v}_k^{\mathrm{pr}} + \mathbf{J}_k^{\mathrm{pr}})\cdot\mathbf{n}_k \,\mathrm{d}a \end{aligned} \quad (5)$$

where

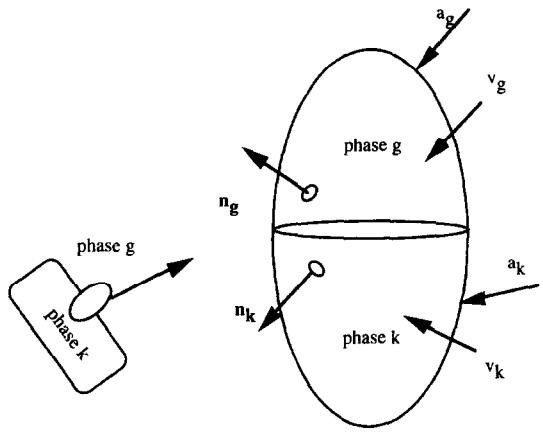

Fig. 3. Sketch of a control volume.

Using Leibnitz's rule and Gauss's theorem to transform this generic equation, and providing that this equation is satisfied at every point and every time, the local instantaneous equations are:

gas phase

$$\frac{\partial}{\partial t}(\rho_g\psi_g) + \nabla\cdot(\rho_g\psi_g\mathbf{v}_g) + \nabla\cdot\mathbf{J}_g - \rho_g\Phi_g = 0 \quad (6)$$

solid phase

$$\frac{\partial}{\partial t}(\rho_k\psi_k) + \nabla\cdot(\rho_k\psi_k\mathbf{v}_k) + \nabla\cdot\mathbf{J}_k - \rho_k\Phi_k = -S_k \quad (7)$$

interface

$$\sum_m [\rho_k\psi_k(\mathbf{v}_I - \mathbf{v}_m)\cdot\mathbf{n}_m - \mathbf{J}_m\cdot\mathbf{n}_m] = \dot{m}_k^{\mathrm{pr}}\psi_k^{\mathrm{pr}} \quad (8)$$

where the rate of mass reduction of phase k due to drying and pyrolysing processes is defined as

$$\dot{m}_k^{\mathrm{pr}} = \rho_k^{\mathrm{pr}}\mathbf{v}^{\mathrm{pr}}\cdot\mathbf{n}_k.$$

Defining, respectively, the rate of gaseous mass addition and the rate of mass reduction of phase k due to surface combustion as

$$\rho_g(\mathbf{v}_I - \mathbf{v}_g)\cdot\mathbf{n}_g = \dot{m}_g \quad (9)$$

$$\rho_k(\mathbf{v}_I - \mathbf{v}_k)\cdot\mathbf{n}_k = -\dot{m}_k^{\mathrm{surf}} \quad (10)$$

it follows that

$$\dot{m}_g = \dot{m}_k^{\mathrm{pr}} + \dot{m}_k^{\mathrm{surf}}. \quad (11)$$

Balance equation	ψ_m	$\mathbf{J}_m$	Φ_m	S_k	ψ_m^{pr}
Mass	1	0	0	$[\Gamma]_k^{\mathrm{pr}}$	1
Chemical species	Y_m^s	$\rho_m Y_m^s \mathbf{V}_m^s$	ω_m^s	$[\Gamma Y^s]_k^{\mathrm{pr}}$	$Y_k^{\mathrm{pr},s}$
Momentum	$\mathbf{v}_m$	$-\bar{\bar{\Pi}}_m$	$\mathbf{F}_m$	$[\Gamma\mathbf{v}]_k^{\mathrm{pr}}$	$\mathbf{v}_k^{\mathrm{pr}}$
Energy	e_m	$\mathbf{q}_m + \mathbf{R}_m - \bar{\bar{\Pi}}_m\cdot\mathbf{v}_m$	$\mathbf{F}_m\cdot\mathbf{v}_m$	$[\Gamma e]_k^{\mathrm{pr}}$	e_k^{pr}

In this last equation, the right-hand terms represent the fuel mass loss rates due to pyrolysis and char combustion, respectively.

2.3. *Multiphase equations*

2.3.1. *Average variables.* In the multiphase approach, the volume for the gas phase, denoted $V_{g\infty}$, is the portion of void volume occupied by the gas while the remaining portion occupied by the particles is considered to be the volume for the N solid phases ($N = 2$ in Fig. 4). Every solid phase k occupies a volume $V_{k\infty}$.

Each solid phase is constituted with p_k^∞ particles. The particle p of the phase k has a volume V_{pk} and a surface S_{pk}, with p varying in the range $1-p_k^\infty$.

Extending the method of Anderson and Jackson [6] to the multiphase case, one can define:

$$\alpha_g(\mathbf{x},t)=\int_{V_{g\infty}} g(r)\,\mathrm{d}v \quad \text{and} \quad \alpha_k(\mathbf{x},t)=\int_{V_{k\infty}} g(r)\,\mathrm{d}v \tag{12}$$

in which $\mathbf{x}$ is the position vector of a point M and r is the distance between M and a remote point M', $\mathrm{d}v$ is a basic volume surrounding M' and $g(r)$ is a weighting function with the following properties:

$$\int_{V_\infty} g(r)\,\mathrm{d}v = 4\Pi\int_{r=0}^{r=\infty} g(r)r^2\,\mathrm{d}r = 1 \tag{13}$$

where

$$V_\infty = V_{g\infty}\cup\left(\sum_{k=1}^{N} V_{k\infty}\right). \tag{14}$$

So, the average properties of the gas phase and a solid phase k are defined by:

$$\alpha_g\langle a_g\rangle(\mathbf{x},t)=\int_{V_{g\infty}} g(r)a_g(\mathbf{y},t)\,\mathrm{d}v \tag{15}$$

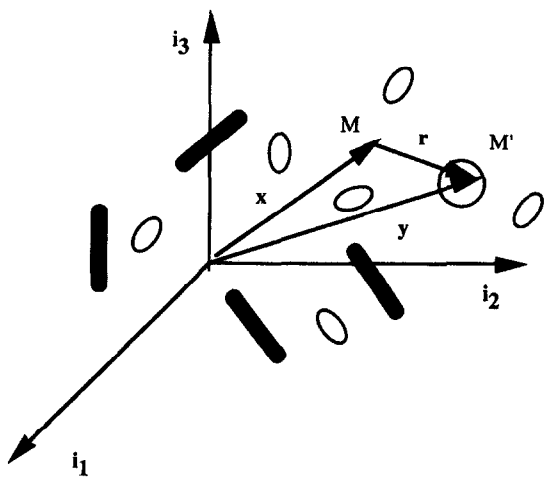

Fig. 4. Schematic representation of the multiphase medium.

$$\alpha_k\langle a_k\rangle(\mathbf{x},t)=\int_{V_{k\infty}} g(r)a_k(\mathbf{y},t)\,\mathrm{d}v = \sum_{p=1}^{p_k^\infty}\int_{V_{pk}} g(r)a_k(\mathbf{y},t)\,\mathrm{d}v \tag{16}$$

in which a_m ($m = g$ or k) is either a scalar function, or the component of a vector or of a second-order tensor.

Remark: If also a_k is considered as constant inside each particle p, we can write:

$$\alpha_k\langle a_k\rangle(\mathbf{x},t)=\sum_{p=1}^{p_k^\infty} g(r_p)a_k(\mathbf{y},t)V_{pk}.$$

2.3.2. *Average equations.* Multiplying the gas balance equation by g and integrating over the region occupied by the gas-phase yields

$$\int_{V_{g\infty}} g\left[\frac{\partial}{\partial t}(\rho_g\psi_g)+\nabla\cdot(\rho_g\psi_g\mathbf{v}_g)+\nabla\cdot\mathbf{J}_g-\rho_g\Phi_g\right]\mathrm{d}v = 0. \tag{17}$$

Using the mathematical theorems of Appendix 1 and after some algebraic manipulations, we obtain

$$\frac{\partial}{\partial t}(\alpha_g\langle\rho_g\psi_g\rangle)+\nabla\cdot(\alpha_g\langle\rho_g\psi_g\mathbf{v}_g+\mathbf{J}_g\rangle)-\alpha_g\langle\rho_g\Phi_g\rangle = \sum_{k=1}^{N}\sum_{p=1}^{p_k^\infty}\int_{S_{pk}} g(\dot{m}_g\psi_g-\mathbf{J}_g\cdot\mathbf{n}_g)\,\mathrm{d}s. \tag{18}$$

Multiplying the balance equation of the phase k by g, integrating over the region occupied by the elementary volume V_{pk}, and summing over all these elementary volumes of the phase k, we have

$$\sum_{p=1}^{p_k^\infty}\int_{V_{pk}} g\left[\frac{\partial}{\partial t}(\rho_k\psi_k)+\nabla\cdot(\rho_k\psi_k\mathbf{v}_k)+\nabla\cdot\mathbf{J}_k-\rho_k\Phi_k\right]\mathrm{d}v = \sum_{p=1}^{p_k^\infty}\int_{V_{pk}} gS_k\,\mathrm{d}v \tag{19}$$

also

$$\frac{\partial}{\partial t}\alpha_k\langle\rho_k\psi_k\rangle+\nabla\cdot\alpha_k\langle\rho_k\psi_k\mathbf{v}_k+\mathbf{J}_k\rangle-\alpha_k\langle\rho_k\Phi_k\rangle = -\alpha_k\langle S_k\rangle-\sum_{p=1}^{p_k^\infty}\int_{S_{pk}} g(\dot{m}_k^{\mathrm{surf}}\psi_k+\mathbf{J}_k\cdot\mathbf{n}_k)\,\mathrm{d}s. \tag{20}$$

Proceeding analogously we find the boundary conditions at the interface between the gas and the solid phase k, namely the average jump conditions, as

$$\sum_{p=1}^{p_k^\infty}\int_{S_{pk}} g(\dot{m}_g\psi_g-\mathbf{J}_g\cdot\mathbf{n}_g)\,\mathrm{d}s = \sum_{p=1}^{p_k^\infty}\int_{S_{pk}} g(\dot{m}_k^{\mathrm{surf}}\psi_k+\dot{m}_k^{\mathrm{pr}}\psi_k^{\mathrm{pr}} +\mathbf{J}_k\cdot\mathbf{n}_k+\mathbf{J}_k^{\mathrm{pr}}\cdot\mathbf{n}_k)\,\mathrm{d}s. \tag{21}$$

2.4. *Gas phase radiative balance equation*

The influences of radiant heat transfer are exerted through the fluxes $\mathbf{J}_m$ in the energy conservation equations of the gas or solid phases. We focus only our attention on the balance of radiative intensity for the gas phase because it will be seen later that solid phases can be considered as opaque media.

Let Ω be the solid angle and L_g^Ω the radiant intensity in the gas phase at a point M in the $\mathbf{e}$ direction (Fig. 5). The radiative flux is defined by [8]

$$\mathbf{R}_g = \int_\Omega L_g^\Omega \mathbf{e}\, \mathrm{d}\Omega. \tag{22}$$

In Cartesian coordinates, it can be shown that

$$\nabla \cdot \mathbf{R}_g = \frac{\partial}{\partial x_i} R_{gi} = \int_\Omega \frac{\partial L_g^\Omega}{\partial x_i} e_i \, \mathrm{d}\Omega \tag{23}$$

with $e_i = \mathbf{e} \cdot \mathbf{i}_i$.

Along the direction $\mathbf{e}$, if the medium is assumed to be grey and non-scattering, the equation for the transfer of thermal radiation can be expressed as

$$\frac{\partial L_g^\Omega e_i}{\partial x_i} = -a_g^\Omega L_g^\Omega + a_g^\Omega L_0^\Omega \tag{24}$$

where a_g^Ω is the gas absorption coefficient and L_0^Ω the black body intensity.

By multiplying by $\boldsymbol{g}$ and integrating over $V_{g\infty}$ and using the previous average definitions and the mathematical theorems (Appendix 1), we have

$$e_1 \frac{\partial \alpha_g \langle L_g^\Omega \rangle}{\partial x_1} + e_2 \frac{\partial \alpha_g \langle L_g^\Omega \rangle}{\partial x_2} + e_3 \frac{\partial \alpha_g \langle L_g^\Omega \rangle}{\partial x_3} + \sum_{k=1}^{N} \sum_{p=1}^{p_k^\alpha} \int_{S_{pk}} \boldsymbol{g} L_g^\Omega \mathbf{n}_g \cdot \mathbf{e}\, \mathrm{d}s = -\alpha_g \langle a_g^\Omega L_g^\Omega \rangle + \alpha_g \langle a_g^\Omega L_0^\Omega \rangle \tag{25}$$

where $\mathrm{d}s$ is an infinitesimal displacement along $\mathbf{e}$.

In this equation, the last term of the left-hand side represents the solid–solid radiative exchanges through the gas phase. The terms of the right-hand side represent the attenuation of intensity by absorption and the increase of intensity by emission in the gas phase. These terms, taken as zero in the following part of this work, can play a very important role in the case of highly absorbing or sooting combustion gases.

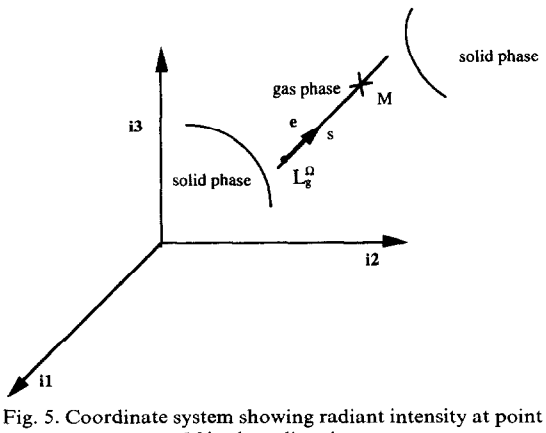

Fig. 5. Coordinate system showing radiant intensity at point M in the $\mathbf{e}$ direction.

3. REDUCED EQUATIONS: A ZEROTH-ORDER MODEL

From the set of equations resulting in a general analysis of the reactive, radiative, and multiphase medium, a simplified approach (called zeroth-order model) is developed with the aim of dissociating the effects of phenomena from those of transfers. This reduced model leads to a qualitative description of fire spread through an heterogeneous medium. It is based on simplifying assumptions and simplified submodels.

The simplifying assumptions have been formulated for each balance equation and their associate submodels.

3.1. *Mass equations*

A first assumption consists of the fact that the solid particles are fixed in space

$$\mathbf{v}_k = 0. \tag{A1}$$

It seems obvious that models in which this assumption is used can be representative of wildland fires.

Char combustion processes require the use of an appropriate kinetic model [9–12], but in the present simplified model, for the sake of clarity, char combustion is neglected (the only combustion process taken into account is that of pyrolysis products in gaseous phase). Thus,

$$\dot{m}_k^{\mathrm{surf}} = 0. \tag{A2}$$

This assumption implies that there is no particle surface regression and no char combustion contribution in the mass, momentum and energy balance equations.

Using [A1] and [A2], eqns (18)–(20) can be written as

$$\frac{\partial}{\partial t}(\alpha_g \langle \rho_g \rangle) + \nabla \cdot (\alpha_g \langle \rho_g \mathbf{v}_g \rangle) = \sum_{k=1}^{N} \alpha_k \langle \sigma_k \dot{m}_g \rangle_1 \tag{26}$$

$$\frac{\mathrm{d}}{\mathrm{d}t}(\alpha_k \langle \rho_k \rangle) = -\alpha_k \langle \sigma_k \dot{m}_k^{\mathrm{pr}} \rangle_1 \tag{27}$$

$$\alpha_k \langle \sigma_k \dot{m}_g \rangle_1 = \alpha_k \langle \sigma_k \dot{m}_k^{\mathrm{pr}} \rangle_1. \tag{28}$$

In order to evaluate mass transfer terms, the quantity $\dot{m}_k^{\mathrm{pr}}$ has to be known. It can be deduced from experimental pyrolysis curves or calculated according to an Arrhenius-type law [10–13]. In this paper, the former technique is used.

To eliminate the complexities of gas flow through the solid material, the pyrolysis products are assumed

to be removed out of the solid instantaneously upon their release. The fact that there is no accumulation of pyrolysis products inside the phase k implies

$$\alpha_k\langle[\Gamma]_k^{\mathrm{pr}}\rangle = \alpha_k\langle\sigma_k\dot{m}_k^{\mathrm{pr}}\rangle. \qquad [A3]$$

3.2. *Chemical species equations—combustion model*

If we further assume that mass diffusion of any chemical species s in the gas phase is neglected and that no chemical reactions occur in solid phase, we get, respectively,

$$\mathbf{V}_m^s = 0 \qquad [A4]$$

$$\omega_k^s = 0. \qquad [A5]$$

Taking into account the assumptions [A1]–[A5], eqns (18)–(20) reduce to

$$\frac{\partial}{\partial t}(\alpha_g\langle\rho_g Y_g^s\rangle)+\nabla\cdot(\alpha_g\langle\rho_g Y_g^s\mathbf{v}_g\rangle) = \sum_{k=1}^{N}\alpha_k\langle\sigma_k\dot{m}_g Y_g^s\rangle_{\mathrm{I}}+\alpha_g\langle\rho_g\omega_g^s\rangle \qquad (29)$$

$$\frac{\mathrm{d}}{\mathrm{d}t}(\alpha_k\langle\rho_k Y_k^s\rangle) = -\alpha_k\langle\sigma_k\dot{m}_k^{\mathrm{pr}}Y_k^{\mathrm{pr},s}\rangle_{\mathrm{I}} \qquad (30)$$

$$\alpha_k\langle\sigma_k\dot{m}_g Y_g^s\rangle_{\mathrm{I}} = \alpha_k\langle\sigma_k\dot{m}_k^{\mathrm{pr}}Y_k^{\mathrm{pr},s}\rangle_{\mathrm{I}} \qquad (31)$$

where the mass fraction of the pyrolysis products at the solid–gas surface are deduced from

$$Y_k^{\mathrm{pr},s} = \frac{\dot{m}_k^{\mathrm{pr},s}}{\sum_{s=1}^{\mathrm{nesp}}\dot{m}_k^{\mathrm{pr},s}}.$$

The combustion process is represented as a single, one-step reaction

$$\mathrm{Fuel}+\mathrm{Oxidant} = \mathrm{Products}.$$

As an example, if fuel is CO, fuel-rich condition ($n_{\mathrm{CO}} > 2n_{\mathrm{O}_2}$) or fuel-lean condition ($n_{\mathrm{CO}} \leqslant 2n_{\mathrm{O}_2}$) can occur locally

$$n_{\mathrm{CO}}\mathrm{CO}+n_{\mathrm{O}_2}\mathrm{O}_2 = \begin{cases} 2n_{\mathrm{O}_2}\mathrm{CO}_2+(n_{\mathrm{CO}}-2n_{\mathrm{O}_2})\mathrm{CO} & \text{(fuel-rich)} \\ n_{\mathrm{CO}}\mathrm{CO}_2+\frac{1}{2}(2n_{\mathrm{O}_2}-n_{\mathrm{CO}})\mathrm{O}_2 & \text{(fuel-lean).} \end{cases}$$

Then, the mass rate of production of species s, ω_g^s, due to the reaction given previously can be easily determined.

3.3. *Momentum equations*

The statement of motionless particles [A1] serves as the momentum balance equations for the solid phase k. In addition, two assumptions commonly used are made, namely:

[A6] viscous gas effects are neglected except at the solid–gas interface;

[A7] the rate of increase of linear momentum of the gas phase due to drying and pyrolysis of the solid phases is neglected:

$$\sum_{k=1}^{N}\alpha_k\langle\sigma_k\dot{m}_g\mathbf{v}_g\rangle_{\mathrm{I}} = 0.$$

In return for which, eqn (18) becomes

$$\frac{\partial}{\partial t}(\alpha_g\langle\rho_g\mathbf{v}_g\rangle)+\nabla\cdot(\alpha_g\langle\rho_g\mathbf{v}_g\mathbf{v}_g\rangle) = \sum_{k=1}^{N}\alpha_k\langle\sigma_k\bar{\bar{\Pi}}_g\cdot\mathbf{n}_g\rangle_{\mathrm{I}}-\nabla\cdot(\alpha_g p\bar{\bar{\mathbf{I}}}) \qquad (32)$$

where

$$\sum_{k=1}^{N}\alpha_k\sigma_k\langle\bar{\bar{\Pi}}_g\cdot\mathbf{n}_g\rangle_{\mathrm{I}} = \sum_{k=1}^{N}0.5n_k\Pi r_k^2\rho_g C_{dk}\mathbf{v}_g|\mathbf{v}_g| = \sum_{k=1}^{N}\frac{3}{8}\frac{\alpha_k}{r_k}\rho_g C_{dk}\mathbf{v}_g|\mathbf{v}_g| = \frac{3}{8}\rho_g\mathbf{v}_g|\mathbf{v}_g|\sum_{k=1}^{N}C_{dk}\frac{\alpha_k}{r_k}$$

where the drag coefficient is deduced from the correlation of Marty [14] for a single solid phase

$$C_{dk} = \frac{12}{Re_k}+\frac{30}{Re_k^2}+\frac{4}{Re_k^{1/2}}$$

and

$$Re_k = \frac{2\rho_g|\mathbf{v}_g|r_k}{\mu_g}.$$

3.4. *Radiative transfer equation*

Assuming that: [A8] the gas phase is treated as a transparent medium, [A9] solid particles act as black bodies, the right-hand side of eqn (25) vanishes and the last term of the left-hand side can be expressed as

$$\sum_{k=1}^{N}\sum_{p=1}^{p_k^\infty}\int_{S_{pk}}\mathbf{g}L_g^\Omega\mathbf{e}\cdot\mathbf{n}_g\,\mathrm{d}s = \sum_{k=1}^{N}\left(\frac{\alpha_k}{4}\langle\sigma_k L_g^\Omega\rangle_{\mathrm{I}}-\frac{\alpha_k}{4\Pi}\langle\sigma_k\beta T_k^4\rangle_{\mathrm{I}}\right) \qquad (33)$$

where β is the Stefan–Boltzman constant and T_k the surface temperature of the solid phase k. Equation (25) can be rewritten as

$$e_1\frac{\partial}{\partial x_1}(\alpha_g\langle L_g^\Omega\rangle)+e_2\frac{\partial}{\partial x_2}(\alpha_g\langle L_g^\Omega\rangle)+e_3\frac{\partial}{\partial x_3}(\alpha_g\langle L_g^\Omega\rangle) = \sum_{k=1}^{N}\left[\frac{\alpha_k}{4\Pi}\langle\sigma_k\beta T_k^4\rangle_{\mathrm{I}}-\frac{\alpha_k}{4}\langle\sigma_k L_g^\Omega\rangle_{\mathrm{I}}\right]. \qquad (34)$$

It is obvious that the assumption of transparent gas phase made previously implies that the divergence of

the radiative flux is zero and consequently radiative terms will vanish in the gas phase energy equation.

3.5. *Energy equation*

As for the energy equation for the solid phase k, by using the jump condition (21), the term related to thermal radiation is expressed as

$$\sum_{p=1}^{p_k^{sc}} \int_{S_{pk}} g \left(\int_{\Omega} L_g^{\Omega} \mathbf{e} \cdot \mathbf{n}_g \, \mathrm{d}\Omega \right) \mathrm{d}s = \alpha_k \langle \sigma_k \mathbf{R}_g \cdot \mathbf{n}_g \rangle_{\mathrm{I}}$$

$$= \int_{\Omega} \sum_{p=1}^{p_k^{sc}} \int_{S_{pk}} (g L_g^{\Omega} \mathbf{e} \cdot \mathbf{n}_g \, \mathrm{d}s) \, \mathrm{d}\Omega. \quad (35)$$

Using eqn (33), we then get

$$\sum_{p=1}^{p_k^{sc}} \int_{S_{pk}} g \left(\int_{\Omega} L_g^{\Omega} \mathbf{e} \cdot \mathbf{n}_g \, \mathrm{d}\Omega \right) \mathrm{d}s$$

$$= \int_{\Omega} \left[\frac{\alpha_k}{4} \langle \sigma_k L_g^{\Omega} \rangle_{\mathrm{I}} - \frac{\alpha_k}{4\Pi} \langle \sigma_k \beta T_k^4 \rangle_{\mathrm{I}} \right] \mathrm{d}\Omega. \quad (36)$$

If we define

$$I_g^{(0)} = \int_{\Omega} L_g^{\Omega} \, \mathrm{d}\Omega$$

we have

$$\int_{\Omega} \left[\frac{\alpha_k}{4} \langle \sigma_k L_g^{\Omega} \rangle_{\mathrm{I}} - \frac{\alpha_k}{4\Pi} \langle \sigma_k \beta T_k^4 \rangle_{\mathrm{I}} \right] \mathrm{d}\Omega$$

$$= \frac{\alpha_k}{4} \sigma_k I^{(0)} - \alpha_k \sigma_k \beta T_k^4. \quad (37)$$

The value of $I^{(0)}$ is obtained from the radiant heat transfer by using the P1-approximation [8] (cf Appendix 2). Due to the radiative properties of the solid particles, we have $\nabla \cdot \alpha_k \langle \mathbf{R}_k \rangle = 0$.

In addition, by neglecting conduction effects except at the interface and the rate of work done by viscous stresses at the interface, and using eqns (34) and (35), eqns (18), (20), and (21) become

$$\frac{\partial}{\partial t}(\alpha_g \langle \rho_g e_g \rangle) + \nabla \cdot (\alpha_g \langle \rho_g e_g \mathbf{v}_g \rangle)$$

$$= \sum_{k=1}^{N} \alpha_k \langle \sigma_g \dot{m}_g e_g \rangle_{\mathrm{I}} - \sum_{k=1}^{N} \alpha_k \langle \sigma_g \mathbf{q}_g \cdot \mathbf{n}_g \rangle_{\mathrm{I}}$$

$$- \nabla \cdot (\alpha_g \langle p_g \mathbf{v}_g \rangle) \quad (38)$$

$$\frac{\mathrm{d}}{\mathrm{d}t}(\alpha_k \langle \rho_k e_k \rangle)$$

$$= -\alpha_k \langle \sigma_k \dot{m}_g e_g \rangle_{\mathrm{I}} + \alpha_k \langle \sigma_g \mathbf{q}_g \cdot \mathbf{n}_g \rangle_{\mathrm{I}}$$

$$+ \int_{\Omega} \left(\frac{\alpha_k}{4} \langle \sigma_k L_g^{\Omega} \rangle_{\mathrm{I}} - \frac{\alpha_k}{4\Pi} \langle \sigma_k \beta T_k^4 \rangle_{\mathrm{I}} \right) \mathrm{d}\Omega \quad (39)$$

$$\alpha_k \langle \sigma_g \dot{m}_g e_g \rangle_{\mathrm{I}} - \alpha_k \langle \sigma_g \mathbf{q}_g \cdot \mathbf{n}_g \rangle_{\mathrm{I}}$$

$$- \int_{\Omega} \left[\frac{\alpha_k}{4} \langle \sigma_k L_g^{\Omega} \rangle_{\mathrm{I}} - \frac{\alpha_k}{4\Pi} \langle \sigma_k \beta T_k^4 \rangle_{\mathrm{I}} \right] \mathrm{d}\Omega$$

$$= \alpha_k \langle \sigma_k \dot{m}_k^{\mathrm{pr}} e_k^{\mathrm{pr}} \rangle_{\mathrm{I}} - \alpha_k \langle \sigma_k \mathbf{q}_k \cdot \mathbf{n}_k \rangle_{\mathrm{I}} + \alpha_k \langle \sigma_k \mathbf{R}_k \cdot \mathbf{n}_k \rangle_{\mathrm{I}}. \quad (40)$$

At the interface, if the exit temperature of pyrolysis products is assumed to be the solid surface temperature T_k, their internal energy is defined by $\langle e_g \rangle_{\mathrm{I}} = e(Y_k^{\mathrm{pr},s}, T_k)$.

The interphase convective heat transfer is related to the flow properties according to the correlation of Yuen and Chen [15], in terms of the Reynolds and Prandtl numbers

$$Nu_k = 2 + 0.6 Re_k^{1/2} \, Pr^{1/3}$$

where

$$Nu_k = \frac{2 h_k r_k}{\lambda_k}$$

and

$$h_k = \frac{\mathbf{q}_g \cdot \mathbf{n}_g}{T_g - T_k}.$$

3.6. *Equations of state*

Internal energy is defined to include the chemical energy

$$e(Y_s, T, p) = \sum_{s=1}^{\mathrm{nesp}} Y_s \left(\Delta h_{fs}^0 + \int_{T_0}^{T} C_{ps}(T) \, \mathrm{d}T \right) - \frac{p}{\rho}. \quad (41)$$

It appears clearly that any chemical composition variation (due to chemical reaction) implies internal energy variations. The equation of state for a multicomponent system based upon ideal-gas assumptions can be written as

$$p = \rho R T \sum_{s=1}^{\mathrm{nesp}} \frac{Y_s}{W_s}. \quad (42)$$

4. NUMERICAL RESOLUTION

One-dimensional simulations are carried out. Therefore, the main dependent variables of the problem are for the gas phase, the velocity v_g, the pressure p, the energy e, the species mass fractions Y_g^s ($s = 1, 2, \ldots,$ nesp), the zeroth moment of the radiant intensity I and for the solid phases ($k = 1, 2, \ldots, N$) the energy e_k, the density ρ_k, the species mass fractions Y_k^s.

All these gas variables, with the exception of p, appear as the subject of differential equations of the general form

$$\frac{\partial}{\partial t}(\alpha_g \rho_g \phi_g) + \frac{\partial}{\partial x}(\alpha_g \rho_g \phi_g v_g) = S_{\phi g} \quad (43)$$

where ϕ_g stands for a generic fluid property, $\phi_g = 1$, Y_g^s ($s = 1, 2, \ldots,$ nesp), v_g, I, e_g, and $S_{\Phi g}$ is the right-

hand term of the equations (26), (29), (32), (A2.3), and (38) written in one-dimensional form. The governing equations are discretized on a staggered non-uniform grid using a finite-volume procedure with a hybrid differencing scheme [16] for the convective terms. The SIMPLEC algorithm [17] is used to solve the coupling between continuity and momentum equations through pressure. The solution of the resulting algebraic equations is obtained by Thomas' algorithm [18]. For the solid phases, the ordinary-differential equations, eqns (27), (30) and (39), are solved explicitly.

5. RESULTS AND DISCUSSION

Computational simulations of one-dimensional fire propagation are presented. Gravitational effects are not considered. Two configurations are presented: forward (Fig. 6a) and reverse fire propagation (Fig. 6b) with respect to the direction of the inlet flow. Inlet conditions and numerical parameters used in the calculations are given in Table 1.

Results concern the thermal degradation of dry wood particles. The rate of gaseous mass addition due to drying and pyrolysing processes for the solid phase k can be expressed as

$$\dot{m}_k^{pr} = \frac{dm_k^{pr}}{dt} = \frac{dm_k^{pr}}{dT_k}\frac{dT_k}{dt}$$

where dm_k^{pr}/dT_k is deduced from the experimental curves given by Calvin and Diehl [19]. Therefore, the knowledge of temperature T_k of phase k is sufficient to determine pyrolysis products flow rate.

Fire is initiated by maintaining particles of the ignition zone at a high level of temperature, about 1500 K, during 5 s. Energy is transferred to the particles close to the ignition zone by radiation and convection. These particles release water, then volatile products of pyrolysis. The composition of the volatile products of pyrolysis is complicated. The combustible gases consist of hydrocarbons or their derivatives and CO and the noncombustible gases consist of CO_2 and H_2O. Nevertheless, always for clarity, the authors, following Grishin [10], have considered only CO and CO_2 as pyrolysis products. Pyrolysis products mass is about 40% of the total mass of a dry wood particle. CO and CO_2 may be considered to have the same mole fraction [20, 21]. Numerical simulations aim at describing such phenomena as transient fire propagation, chemical mechanisms induced by fuel thermal degradation, radiative and convective effects on fire spreading, and multiphase effects. The results we get are not really relevant, but at this step they reveal the capability of the present formulation in describing fire propagation in a multiphase medium.

Table 1

Length of the domain	1.4 m
Gas phase	
Void fraction, α_g	0.99
Specific heat for all species	1300 J kg^{-1} K^{-1}
Solid phase (dry wood particles)	
Ignition temperature	423 K
Density	680 kg m^{-3}
Specific heat	1337 J kg^{-1} K^{-1}
Surface to volume ratio, σ_k	4285 m^{-1}*
Inlet flow conditions	
$T_{in} = 350$ K	$(Y_{O_2})_{in} = 0.232$
	$(Y_{N_2})_{in} = 0.768$
Initial conditions	
$T_0 = T_{p0} = 350$ K	$(Y_{O_2})_0 = 0.232$
$p_0 = 1.01325 \times 10^5$ Pa	$(Y_{N_2})_0 = 0.768$
Ignition zone	
Location from the left end	from 0.025 to 0.075 m
Other data	
$\mu = 15 \times 10^{-6}$ N s m^{-2}	
$Pr = 0.71$	
Number of grid points	300

* This value corresponds to the Pinus Pinaster needle [25].

5.1. *Two-phase configuration*

5.1.1. *Transient fire propagation.* In Fig. 7(a), the pyrolysis zone trajectories have been plotted in a reverse configuration for three values of the inlet mass flow rate, namely $\dot{m}_{in} = 0.05, 0.1, 0.3$ kg m^{-2} s^{-1}. The location of the ignition zone and the ignition duration are represented schematically in the figure by a grey rectangle. The first evidence is that the thickness of the pyrolysis zone increases as the inlet mass flow rate increases.

For the lower mass flow rate, fire propagates through the entire fuel bed. A steady-state is reached and the final average propagation velocity is about 0.04 m s^{-1}. For $\dot{m}_{in} = 0.1$ kg m^{-2} s^{-1}, fire propagates but slows down from about 10 s and finally stops 20 s later at about 1 m from the left end of the duct. For

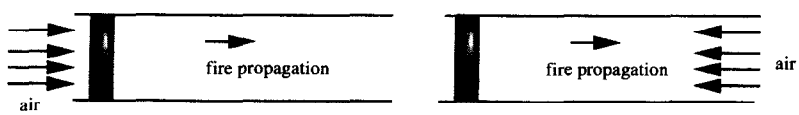

(a) : forward configuration (b) : reverse configuration

Fig. 6. Schematic representation of (a) forward and (b) reverse fire propagations.

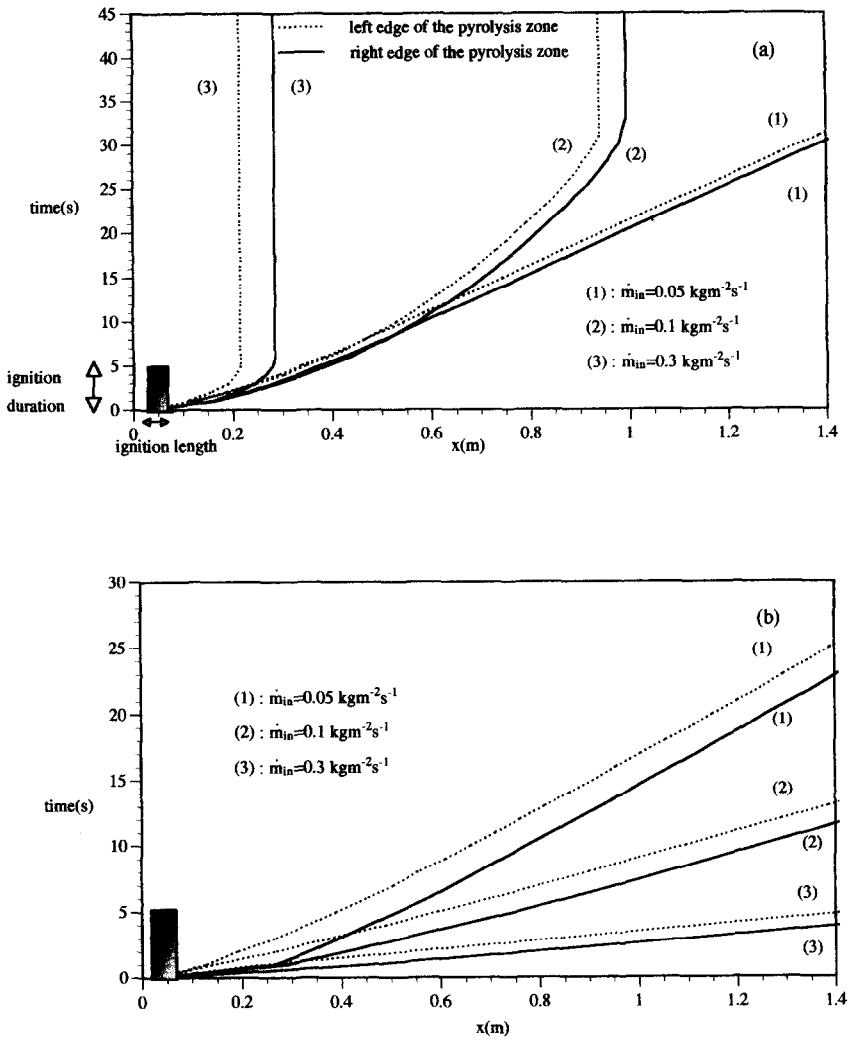

Fig. 7. Pyrolysis zone trajectories for (a) reverse and (b) forward fire propagations.

the higher mass flow rate, fire propagates and stops when ignition ends.

Figure 7(b) shows the pyrolysis zone trajectories in the case of forward fire propagation for the same inlet mass flow rates as previously. In all cases, a steady-state fire propagation is obtained with the following velocities: 0.048, 0.095 and 0.29 m s^{-1} for increasing values of $\dot{m}_{in}$. Contrary to the previous configuration, the thickness of the pyrolysis zone is all the greater as the inlet mass flow rate is smaller.

5.1.2. *Chemical effects.* To explain pyrolysis-induced chemical mechanisms, profiles of CO and CO_2 mass fractions are shown in Fig. 8. They correspond to the lower inlet mass flow rate of the reverse configuration at $t = 26$ s. In these simulations, it is assumed that dry wood particles generate only CO and CO_2, and CO reacts with oxygen of air to give CO_2. CO_2 generation is then the result of both pyrolysis process and chemical reaction. Incoming from the right end of the duct ($x = 1.4$ m), oxygen mass fraction drops suddenly as soon as it reacts with CO resulting from the thermal degradation of particles. Behind the pyrolysis zone, profiles of CO and CO_2 reach a plateau. In this particular reverse configuration, chemical reactions lead to a complete oxygen consumption (underoxidized reaction). Smouldering combustion cannot occur because of the lack of oxygen as observed by Ohlemiller and Lucca [22] in the case of reverse smouldering. Consequently, assumption [A2] seems to be valid.

5.1.3. *Convective and radiative contributions.* As mentioned in the Introduction, energy heat transfer is the main mechanism of fire propagation. Diagram a of Figs 9 and 10 represent, respectively, the steady-state profiles of convective and radiative fluxes for both reverse and forward propagations with an inlet mass flow rate of 0.05 kg m^{-2} s^{-1}. Diagram b shows the profiles of temperature for both phases in the same conditions.

In the reverse propagation configuration [Fig. 9(a)], in front of the pyrolysis zone and behind, convective and radiative effects are competing. In front of the

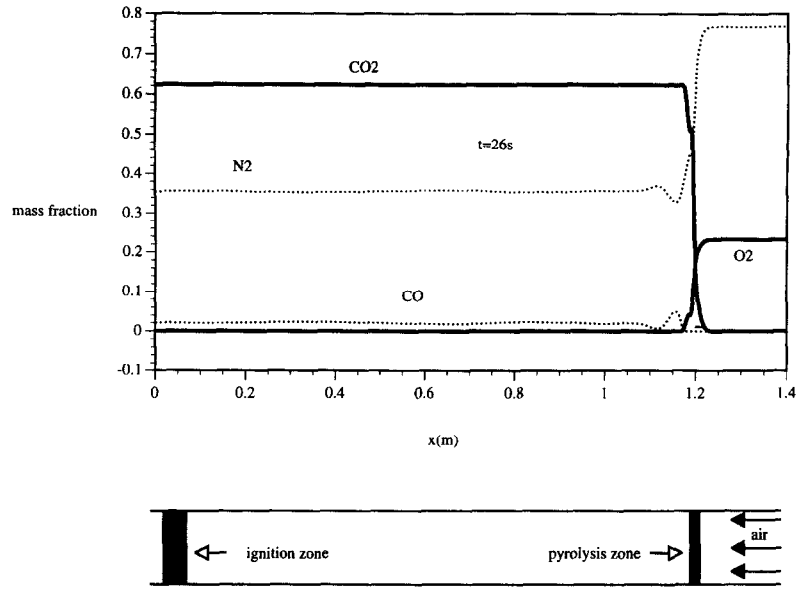

Fig. 8. Mass-fraction profiles in a reverse configuration.

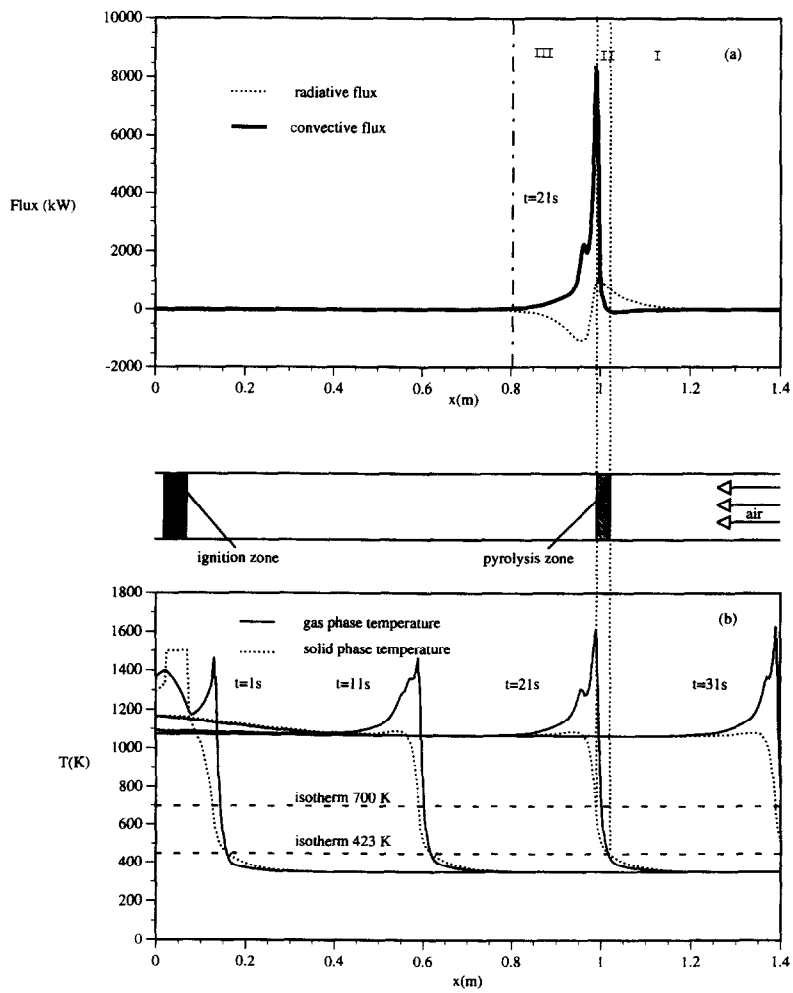

Fig. 9. Steady-state profiles of (a) radiative and convective fluxes, and (b) temperature of gas and solid phases in a reverse configuration.

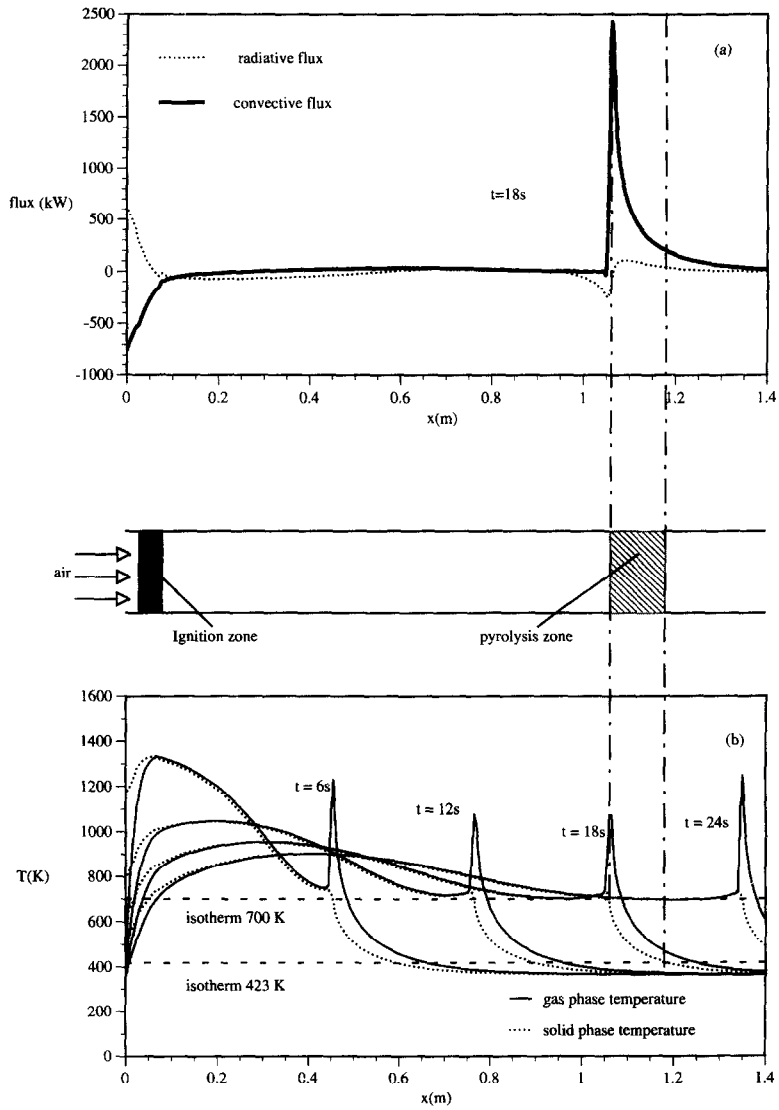

Fig. 10. Steady-state profiles of (a) radiative and convective fluxes, and (b) temperature of gas and solid phases in a forward configuration.

pyrolysis zone (Region I), radiation effects are predominant. That explains why the particle temperature is slightly higher than the gas temperature [Fig. 9(b)]. Behind the pyrolysis zone (Region II), over a distance of 0.1 m, convective effects are now predominant due mainly to the chemical energy release. Immediately behind (Region III), radiative losses prevail over the positive convective contribution. Solid-phase temperature then decreases. The two phases reach an equilibrium temperature of 1075 K when energy fluxes tend to zero. It is obvious that radiation is the main mode of energy transfer in controlling fire propagation velocity for reverse configuration [22]. For the forward propagation configuration (Fig. 10), convective energy transfer is ever greater than the radiative one [Fig. 10(a)]. In front of the pyrolysis zone and inside it, fluxes, mainly the convective one [22], contribute to increasing both solid and gas temperatures. Gas temperature is ever higher than particle temperature [Fig. 10(b)]. Just behind the pyrolysis zone, temperature of both phases diminishes owing to the fact that radiative losses have the edge on convective supply. In such configuration, and unlike the reverse one, fire will propagate in the absence of radiation.

5.1.4. *Regime diagram.* For the reverse configuration, the computed regime diagram is shown in Fig. 11, and represents the variations of propagation speed and maximum solid-phase temperature [Fig. 9(a)] with respect to the inlet mass flow rate. The two curves admit a maximum at $\dot{m}_{in} = 0.064$ kg m^{-2} s^{-1}. Two different regimes appear corresponding, respectively, to an oxygen-limited regime and to a fuel-limited regime as suggested by Fatehi and Kaviany [9]. In

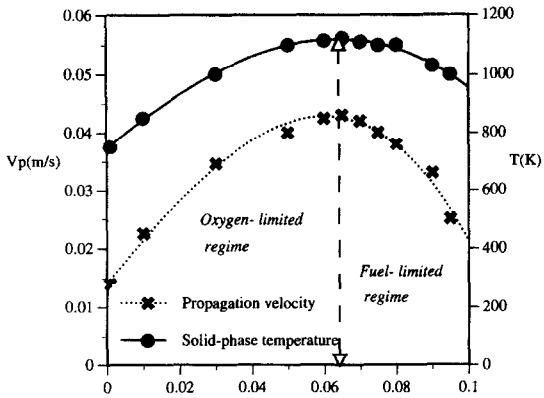

Fig. 11. Variations of solid-phase temperature and propagation velocity with the inlet mass flow rate for the oxygen-limited and fuel-limited regimes in the case of reverse propagation.

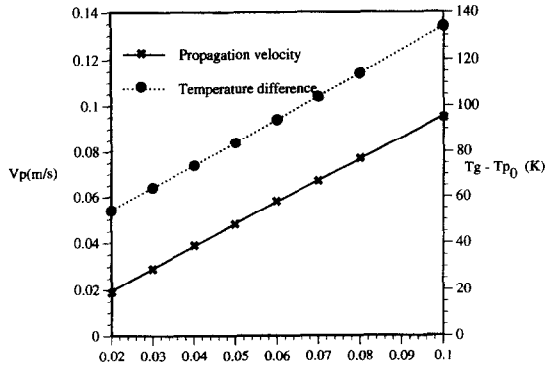

Fig. 12. Variations of the temperature difference $(T_g - T_{p0})$ and propagation velocity with the inlet mass flow rate for the oxygen-limited regime in the case of forward propagation.

accordance with the results of this previous paper, we observe that, within the oxygen-limited regime, increasing the inlet mass flow rate, and then the oxygen supply, causes chemical energy release to increase. The maximum value of the solid-phase temperature behind the pyrolysis zone rises, which in turn enhances radiative transfers to the unburnt fuel particles. It results in higher propagation velocity, as shown experimentally by Ohlemiller and Lucca [22]. One must notice that the behaviour in the oxygen-limited regime presented here is similar to that presented in the case of reverse smouldering by Dosanjh *et al.* [23], Ohlemiller and Lucca [22]. Beyond a critical inlet mass flow rate, CO oxidation is complete. Within this fuel-limited regime, increasing the fresh air mass flow rate causes a cooling convective effect which in turn leads to a diminution of the fire propagation velocity, as pointed out by Fatehi and Kaviany [9]. The maximum propagation velocity is obtained for stoichiometric burning [9]. While the assumption [A2] is valid in the oxygen-limited regime, it is expected to be questionable for the fuel-limited regime [22].

In the case of forward propagation, an oxygen-limited regime is obtained whatever the inlet mass flow rate is. Figure 12 shows the variations of the propagation velocity and temperature difference $T_g - T_{p0}$ with respect to the air mass flow rate in the case of forward propagation. T_g represents the gas temperature at the right edge of the pyrolysis zone where $T_p = T_{ign}$ and T_{p0}, the initial particle temperature. The temperature difference $T_g - T_{p0}$ is a convenient quantity to illustrate the predominance of the convective effects on the propagation process. Figure 12 exhibits the linear dependence of V_p and $T_g - T_{p0}$ on the inlet mass flow rate. A similar behaviour has been previously obtained for thick PMMA by Fernandez-Pello [24].

5.2. *Multiphase configuration*

The influence of the presence of several solid phases (or families) in the heterogeneous medium on the propagation velocity is investigated. For better understanding, only two different families are taken into account. They may differ by the surface/volume ratio and/or the moisture content and/or the pyrolysis products content. In addition, an equivalent model is constructed by considering only one family composed of particles having average properties.

For both multiphase (the gas phase and two solid phases) and equivalent (the gas phase and an equivalent solid phase) models, the volume occupied by the combustible medium and the contact surfaces between wood particles and the gas phase have to be the same. The average surface to volume ratio for the equivalent model is deduced from V_{eq} and S_{eq} defined by

$$n_{eq} V_{eq} = \sum_{k=1}^{2} n_k V_k$$

$$n_{eq} S_{eq} = \sum_{k=1}^{2} n_k S_k. \tag{44}$$

5.2.1. *Sensitivity to surface/volume ratio.* The two solid phases are composed of wood particles with 10 wet% water content. Only surface to volume ratio varies from one solid phase to the other, $\sigma_1 = 3000$ m^{-1} and $\sigma_2 = 750$ m^{-1}. The inlet mass flow rate is $\dot{m}_{in} = 0.01$ kg m^{-2} s^{-1}. The global packing ratio of the combustible medium, $\alpha_p = \alpha_1 + \alpha_2$, is equal to 0.01. Fire front trajectories for different values of (α_1, α_2) and the equivalent model $(\alpha_{eq} = \alpha_p)$ are given in Fig. 13. It is interesting to note that for $(\alpha_1, \alpha_2) = (0.001, 0.009)$, predicted propagations are quite different. For the multiphase model, fire propagates over 0.4 m then it slows down to finally go on propagating all along the duct. On the contrary, with the equivalent model, fire starts to propagate and stops at about $x = 0.525$ m. For other values of (α_1, α_2), fire propagates and both models predict nearly the same propagation velocities. Other simulations have been carried out by varying the inlet mass flow rate and/or the surface to volume ratio. In most cases, discrepancies between predicted propagation vel-

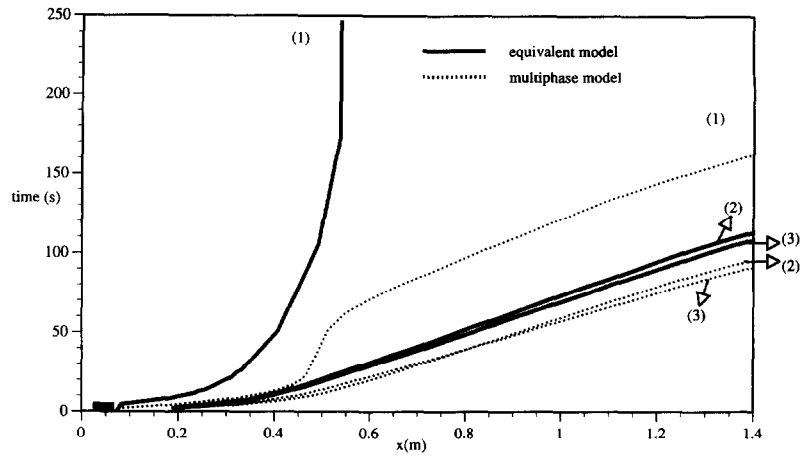

Fig. 13. Fire front trajectories for both multiphase and equivalent models.

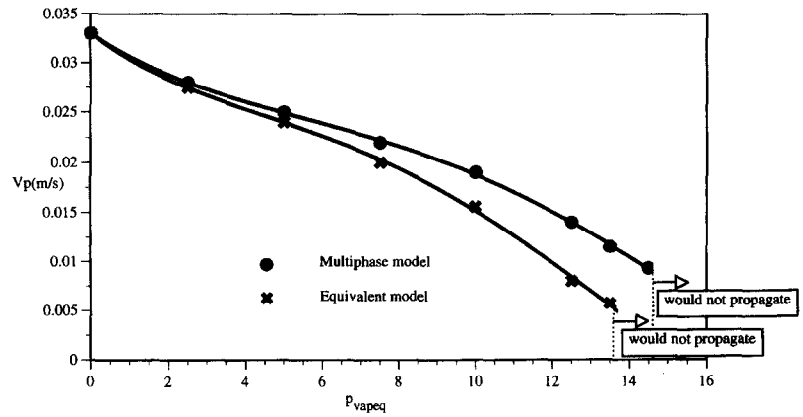

Fig. 14. Variation of the propagation velocities predicted by both multiphase and equivalent models with moisture content.

ocities are not significant even if transient behaviour to steady state may be different.

5.2.2. *Sensitivity to moisture content.* For wet wood particles, a drying process takes place and the production rate of H_2O depends on the moisture content defined as the ratio of the weight of water absorbed to the weight of dry wood. The behaviour of a medium composed of dry and wet wood particles is analysed. To model such a problem, two families with the same surface/ volume ratio $\sigma_1 = \sigma_2 = 4285\ m^{-1}$ and the same packing ratio $\alpha_1 = \alpha_2 = 0.005$ are considered. They differ only from the moisture content level, p_{vap1} for the first family, $p_{vap2} = 0$ for the second one. For the equivalent model, wet wood particles have an average moisture content $p_{vapeq} = 0.5p_{vap1}$.

The relationship between propagation velocities and equivalent moisture contents in the range 0–0.15 is plotted in Fig. 14 for both models. Obviously, increasing moisture content results in decreasing propagation velocity because less heat is available to sustain the mass burning process. For small values of moisture content, propagation velocities are approximately the same for both models, but discrepancies appear for values of the moisture content greater than 0.02. Multiphase models predict higher propagation velocities than the equivalent model. For a moisture content value of 14.5, fire propagates with the multiphase model but does not propagate with the equivalent model. So, the relevance of a multiphase model appears to be incontestable in such cases.

5.2.3. *Sensitivity to surface/volume ratio and pyrolysis product content.* Two families of dry wood particles are considered. the conjugate influence of surface/volume ratio and pyrolysis product content on fire propagation is examined. The corresponding multiphase configuration is

Family 1:		
$\sigma_1 = 4285\ m^{-1}$	$\alpha_1 = 0.005$	p_{pyr1}
Family 2:		
$\sigma_2 = 1500\ m^{-1}$	$\alpha_2 = 0.005$	p_{pyr2}
Equivalent model:		
σ_{eq} [from eqns (44)]	$\alpha_{eq} = 0.01$	$p_{pyreq} = 0.5$ $(p_{pyr1} + p_{pyr2})$

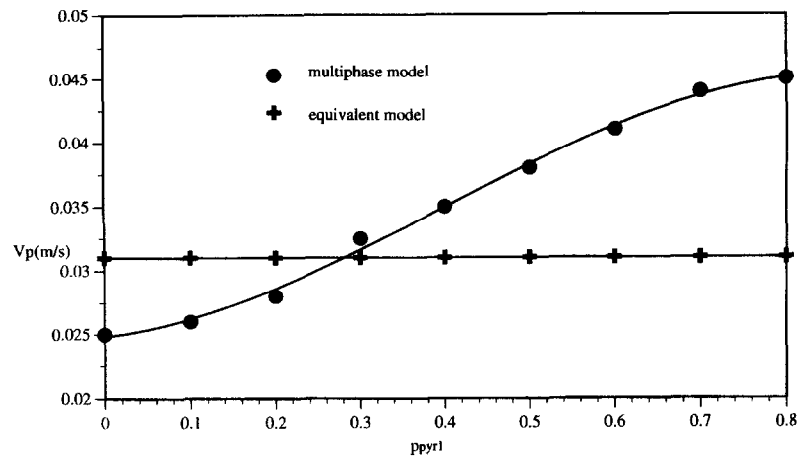

Fig. 15. Variation of the propagation velocities predicted by both multiphase and equivalent models with pyrolysis product distribution.

where the total pyrolysis product content $p_{pyr} = p_{pyr1} + p_{pyr2}$ is equal to 0.08.

Figure 15 shows the evolution of the propagation velocities for both multiphase and equivalent models vs the pyrolysis products content of the family 1, p_{pyr1}. Obviously, the equivalent model gives the same solution whatever p_{pyr1} is. For the multiphase model, propagation velocity increases as p_{pyr1} is increased (and so p_{pyr2} is decreased since the total pyrolysis product content is constant) because more heat is available. Burning intensity is all the greater as pyrolysis products are preferentially distributed into the family of small particles, namely family 1 (highest surface to volume ratio). Discrepancies between the two models are significant and may reach about 40% for the propagation velocity when family 1 contains all the pyrolysis products.

6. CONCLUSION

Extending the mathematical approaches of Delhaye and Anderson and Jackson, a general set of equations has been obtained for describing the fire-induced behaviour of a multiphase, reactive and radiative medium. Using the same averaging procedure, a directional radiative transfer equation for a multiphase medium has been derived. One-dimensional simulations based on a zeroth-order model have been carried out. Reverse and forward fire propagations through an heterogeneous medium composed of fixed particles have been investigated. Despite the simplified nature of the zeroth-order model, it permits to recover some well-known phenomena. In the conditions of the present study, different phenomena have been pointed out.

(1) Based on an unsteady description of reverse propagations, for high inlet mass flow rates, fire does not propagate. Forward fire propagations take place whatever the inlet mass flow rate is.

(2) In reverse configuration, radiation is the mainspring of the fire propagation while in the case of forward propagation, the main mechanism of fire propagation is convection.

(3) In the case of reverse propagation, numerical results obtained reveal the existence of two regimes: an oxygen-limited regime for low inlet mass flow rates and a fuel-limited regime for high rates. Propagation velocity reaches a maximum value for stoichiometric burning. For the oxygen-limited regime, an increase in the air flow rate increases the propagation velocity. In the fuel-limited regime, the propagation velocity decreases as the air flow rate is increased.

(4) In the frame of the multiphase approach, the presence of two solid families in a combustible medium has been examined. Multiphase results are compared to those obtained from an equivalent model. They reveal the great sensitivity of the multiphase model to the surface to volume ratio, moisture content, and pyrolysis product distribution. Discrepancies between the multiphase and the equivalent models can be significant, sometimes up to 50%. In addition, it is found that under certain conditions, a multiphase model predicts a steady fire propagation, whereas there is no propagation using the equivalent model.

Additionally, more realistic predictions might be achieved when further modifications are made on including smouldering combustion, diffusion of chemical species, temperature profile inside the solid particles, and gravitational effects.

A quasi two-dimensional model is under development to emphasize the influence of gravitational effects on fire propagation. Both zeroth-order and quasi 2D models should be validated in the near future.

Acknowledgment—The European Commission is gratefully

acknowledged for providing partial funding for this research in the frame of the EFAISTOS Project.

REFERENCES

1. Weber, R. O., Modeling fire spread through fuel bed. *Progress in Energy and Combustion Science*, 1990, **17**, 67–82.
2. Thomas, P. H., Some aspects of the growth and spread of fire in the open. *Forestry*, 1967, **40**, 139–164.
3. Weber, R. O., Analytical models for fire spread due to radiation. *Combustion and Flame*, 1989, **78**, 398–408.
4. Albini, F. A., A model for fire spread in wildland fuels by radiation. *Combustion Science Technology*, 1985, **42**, 229–258.
5. Delhaye, J. M., Local instantaneous equations—instantaneous space—averaged equations—two-phase flows and heat transfer. *Proceedings of NATO Advanced Study Institute*, Istambul, Vol. 1, 1976.
6. Anderson, T. B. and Jackson, R., A fluid mechanical description of fluidized bed. *Industrial Engineering Chemistry Fundamentals*, 1967, **6**, 527–539.
7. Gough, P. S. and Zwarts, F. J., Modeling heterogeneous two phase reacting flow. *AIAA Journal*, 1979, **17**, 17–25.
8. Siegel, R. and Howell, J. R., *Thermal Radiation Heat Transfer*, 3rd edn. Hemisphere Publishing Corporation, New York, 1992.
9. Fatehi, M. and Kaviany, K., Adiabatic reverse combustion in a packed bed. *Combustion and Flame*, 1994, **99**, 1–17.
10. Grishin, A. M., Zverev, V. G. and Shevelev, S. V., Steady-state propagation of top crown forest-fire. *Fizika Goreniya i Vzryva*, 1986, **22**(6), 101–108.
11. Grishin, A. M., Gruzin, A. D. and Zverev, V. G., Study of the structure and limits of propagation of the front of an upstream forest fire. *Fizika Goreniya i Vzryva*, 1985, **21**(1), 11–21.
12. Nakabe, K., McGrattan, K. B., Kashiwagi, T., Baum, H. R., Yamashita, H. and Kushida, G., Ignition and transition to flame spread over a thermally thin cellulosic sheet in a microgravity environment. *Combustion and Flame*, 1994, **98**, 361–374.
13. Drysdale, D., *An Introduction to Fire Dynamics*. Wiley, New York, 1992.
14. Marty, M., Contribution à l'étude des coefficients de traînée entre phases avec prise en compte d'un transfert de masse. Ph.D. thesis, Marseille, France, 1994.
15. Yuen, M. C. and Chen, L. W., Heat transfer measurements of evaporating liquids droplets. *International Journal of Heat and Mass Transfer*, 1977, **21**, 537–542.
16. Van Doormaal, J. P. and Raithby, G. D., Enhancements of the SIMPLE method for predicting incompressible fluid flows. *Numerical Heat Transfer*, 1984, **7**, 147–163.
17. Patankar, S. V., *Numerical Heat Transfer and Fluid Flow*, Series in Computational Methods in Mechanical and Thermal Science. Hemisphere Publishing Corporation, New York, 1980.
18. Anderson, D. A., Tannehill, J. C. and Fletcher, R. H., *Computational Fluid Mechanics and Heat Transfer*, Series in Computational Methods in Mechanics and Thermal Science. McGraw-Hill, New York, 1984.
19. Calvin, K. L. and Diehl, J. R., Combustion of irradiated dry and wet oak. *Combustion and Flame*, 1981, **42**, 123–138.
20. Farel, P. V., Springer, G. and Vest, C. M., Natural convection boundary layers adjacent to pyrolyzing surfaces. *Combustion and Flame*, 1983, **54**, 1–14.
21. Chan, W. C., Kelbon, M. and Krieger, B. B., Modelling and experimental verification of physical and chemical processes during pyrolysis of a large biomass particle. *Fuels*, 1985, **64**.
22. Ohlemiller, T. J. and Lucca, D. A., An experimental comparison of forward and reverse smolder propagation in permeable fuel beds. *Combustion and Flame*, 1983, **54**, 131–147.
23. Dosanjh, S. S., Pagni, P. J. and Fernandez-Pello, A., Forced cocurrent smoldering combustion. *Combustion and Flame*, 1987, **68**, 131–147.
24. Fernandez-Pello, A., *Combustion Fundamentals of Fire*, ed. G. Cox. Academic Press, New York, 1985, Chapter 2, pp. 31–100.

APPENDIX 1

Mathematical theorems

The use of the weighting function leads to a multiphase formulation of Leibnitz's rule and Gauss's theorem. For the gas phase

$$\int_{V_{g\infty}} g\frac{\partial a_g}{\partial y_i}\,\mathrm{d}v = \frac{\partial}{\partial x_i}(\alpha_g\langle a_g\rangle) + \sum_{k=1}^{N}\sum_{p=1}^{p_k^\infty}\int_{S_{pk}} g n_i a_g\,\mathrm{d}s$$

and

$$\int_{V_{g\infty}} g\frac{\partial a_g}{\partial t}\,\mathrm{d}v = \frac{\partial}{\partial t}(\alpha_g\langle a_g\rangle) - \sum_{k=1}^{N}\sum_{p=1}^{p_k^\infty}\int_{S_{pk}} g a_g(\mathbf{v}_i\cdot\mathbf{n})\,\mathrm{d}s$$

in which $\mathbf{v}_i$ is the local velocity at S_{pk}.

For the solid phase k

$$\sum_{p=1}^{p_k^\infty}\int_{V_{pk}} g\frac{\partial a_k}{\partial y_i}\,\mathrm{d}v = \frac{\partial}{\partial x_i}(\alpha_k\langle a_k\rangle) + \sum_{p=1}^{p_k^\infty}\int_{S_{pk}} g n_i a_k\,\mathrm{d}s$$

$$\sum_{p=1}^{p_k^\infty}\int_{V_{pk}} g\frac{\partial a_k}{\partial t}\,\mathrm{d}v = \frac{\partial}{\partial t}(\alpha_k\langle a_k\rangle) + \sum_{p=1}^{p_k^\infty}\int_{S_{pk}} g a_k(\mathbf{v}_i\cdot\mathbf{n})\,\mathrm{d}s.$$

Moreover, in order to express solid–gas interaction terms and assuming that the function g varies little over the interior of a single particle, we can write [6] for any property A and using the remark given above

$$\sum_{p=1}^{p_k^\infty}\int_{S_{pk}} g(r)A(\mathbf{y},t)\,\mathrm{d}s \approx \sum_{p=1}^{p_k^\infty} g(r_p)\int_{S_{pk}} A(\mathbf{y},t)\,\mathrm{d}s$$

$$= \sum_{p=1}^{p_k^\infty} g(r_p)S_{pk}A_p$$

$$= \sum_{p=1}^{p_k^\infty} g(r_p)V_{pk}(\sigma_k A_p) \approx \alpha_k\langle\sigma_k A\rangle.$$

The conjugate action of the two topological parameters α_k and σ_k is so pointed out.

APPENDIX 2

P1-approximation for the radiative transfer equation

The P1 approximation consists of integrating the radiative transfer equation (34) over all solid angles and expressing radiative intensity as a mathematical series of spherical harmonics. The main interest of this method stays in separating space dependence from directional dependence of the radiant intensity L_Ω^g.

First, eqn (34) can be replaced by an equation involving momentum of the zeroth, first and second-order, namely defined as:

$$I_g^{(0)} = \int_0^{4\pi} L_g^\Omega(S,\Omega)\,\mathrm{d}\Omega$$

$$I_g^{(i)} = \int_{\omega=0}^{4\Pi} e_i L_g^{\Omega}(S,\Omega)\,\mathrm{d}\Omega$$

$$I_g^{(ij)} = \int_{\omega=0}^{4\Pi} e_i e_j L_g^{\Omega}(S,\Omega)\,\mathrm{d}\Omega.$$

Closure relations of the P1 approximation are [8]:

$$I_g^{(ij)} = \tfrac{1}{3}\delta_{ij} I_g^{(0)}. \tag{A2.1}$$

Multiplying the radiative transfer eqn (34) by every direction cosine e_i and then integrating over all solid angles, it follows, after some algebraic manipulations, that

$$\frac{\partial L_g^{\Omega} I_g^{(ij)}}{\partial x_j} = -\sum_k \left[\alpha_k \left\langle \frac{\sigma_k}{4} \right\rangle\right] I_g^{(i)}. \tag{A2.2}$$

There are as many equations as direction cosines.

Integrating the radiative transfer equation (34) over all solid angles, using relations (A2.1) and (A2.2), we have

$$\sum_i \frac{\partial}{\partial x_i}\left[\alpha_g \frac{\partial}{\partial x_i}(\alpha_g I_g^{(0)})\right] = -3\left(\sum_{k=1}^{N} \frac{\alpha_k}{4}\sigma_k\right)\left(\sum_{k=1}^{N} \alpha_k \sigma_k \beta T_k^4 - \sum_{k=1}^{N} \frac{\alpha_k}{4}\sigma_k I_g^{(0)}\right). \tag{A2.3}$$

The field of zeroth-order moment $I_g^{(0)}$ can be easily computed from this equation. Local values are then introduced in the energy equation of solid particles.